Supplemental Information for:

Summertime productivity and carbon export potential in the Weddell Sea, with a focus on the waters adjacent to Larsen C Ice Shelf

RF Flynn[1*], TG Bornman[2,3], JM Burger[1], S Smith[1], KAM Spence[1] and SE Fawcett[1,4]

[1]Department of Oceanography, University of Cape Town, Cape Town, South Africa
[2]South African Environmental Observation Network, Elwandle Coastal Node, Port Elizabeth, South Africa
[3]Institute for Coastal and Marine Research, Nelson Mandela University, Port Elizabeth, South Africa
[4]Marine and Antarctic Research centre for Innovation and Sustainability (MARIS), University of Cape Town, Cape Town, South Africa

[*]Corresponding author: Raquel Flynn (flyraq001@myuct.ac.za)

This supporting information document provides ancillary methodological detail pertaining to (1) the carbon content of the diatom species identified using Light Microscopy, (2) the identification of phytoplankton groups using flow cytometry and (3) estimates of urea uptake for the purposes of computing total nitrogen consumption relative to net primary production (NPP). It additionally includes two supplemental figures and two supplemental tables.

Supporting Text

S1. Carbon content of the identified Antarctic diatom species

Light Microscopy was used for the identification of the diatom cells to the lowest taxonomic classification possible. Due to unforeseen circumstances, we were unable to the measure the size and carbon content of the individual diatom species. We therefore used the average size (µm) and carbon content (pg C $cell^{-1}$) for the diatom species identified in the study as determined by Leblanc et al. (2012) for high latitude locations (50 – 70°S) (Table S1).

S2. Flow cytometric identification of phytoplankton populations

Flow cytometry was used to identify the various phytoplankton populations at all stations sampled. The size-class of each cell was determined based on forward scatter area (FSC-A) relative to the FSC-A of 2.8 µm and 20 µm beads (Figure S1a). Once categorised as picoplankton (<2.8 µm), nanoplankton (2.8-20 µm) or microplankton (>20 µm), the cells were further subdivided into six populations based on their Phycoerythrin (PE) fluorescence relative to their chlorophyll-a fluorescence (Figure S1b).

Synechococcus (Syn) fluoresce with high PE and relatively low chlorophyll-a. In this study, two Syn populations were identified, with the one population having a lower PE content (Syn 2) relative to the other (Syn 1; Figure S1b). We note that the Syn populations were not identified based on their size but rather only using PE vs. chlorophyll-a. This is because, as Figure S1a shows, the Syn populations had FSC-A values that ranged across the pico- and nanoplankton size-classes. This is an artefact of Syn having a high ratio of photosystem I to photosystem II compared to the other phytoplankton populations, which acts to increase the electron chain activity, leading to an increase in the emission spectrum and low excitation of the Syn populations (Kaprelyants and Kell 1993; Sunda and Huntsman 2015).

The picoeukaryotes (PicoEuk), nanoeukaryotes (NanoEuk) and microeukatyores (MicroEuk) were initially identified based on their FSC-A relative to the FSC-A of the 2.8 µm and 20 µm beads (Figure S1a). In additions to FSC-A, PicoEuk and NanoEuk are generally characterized by intermediate chlorophyll-a fluorescence and low PE fluorescence relative to the other phytoplankton groups (Figure S1b). The PicoEuk and NanoEuk 2 population fluoresced similarly, with their only discerning factor being size, while the NanoEuk 1 population had relatively higher PE and chlorophyll-a fluorescence. The MicroEuk population had high PE fluorescence and variable chlorophyll-a fluorescence. Due to the low abundance of the microplankton, all cells >20 µm were defined as MicroEuk.

To determine the average biovolume of each phytoplankton groups, six spherical beads of varying diameters (ranging from 1-15 µm) were run on the flow cytometer. A calibration curve of FSC-A versus volume was used to estimate the biovolume of the various phytoplankton populations (Figure S1c; Table S2). Due to the anomalous FSC-A of the Syn populations, the average biovolume for these populations was taken from literature (Kana and Glibert 1987; Paulsen et al. 2015).

S3. Including urea uptake in estimates of total nitrogen uptake

If NPP is mainly supported by NO_3^- and NH_4^+ and phytoplankton growth is balanced, the total N uptake rate (i.e., $\rho N_x = \rho NO_3^- + \rho NH_4^+$) at a given station multiplied by the Redfield C:N ratio (6.63) should approximate NPP at that station (e.g., Peng et al. 2018, Mdutyana et al. 2020, others). For the summertime Weddell Sea, NPP was generally accounted for by $\rho NO_3^- + \rho NH_4^+$ only, with N uptake x 6.63 even exceeding NPP at some of the AP and WG stations (by 142 ± 234% on average; Figure S2, black symbols). At some of the stations where urea uptake was directly measured (i.e., at LCIS and WG1), it appears that ρurea was stimulated (i.e., total N uptake (= $\rho NO_3^- + \rho NH_4^+$ + ρurea) x 6.63 exceeds NPP when ρurea is included; Figure S2, grey symbols), likely due to the low ambient concentrations of urea-N present in the euphotic zone at the time of sampling (average of 0.2 ± 0.1 µM; Figure 3b and Table 1), such that our ^{15}N-urea additions constituted 56 ± 21% of the combined tracer+ambient urea-N pool. Nonetheless, we cannot discount the possibility of urea supporting some fraction of NPP, which has implications for estimating carbon export potential given that urea is a

regenerated N form. At the stations where urea uptake was measured (11 out of 19), ρurea accounted for 8 ± 6% of total N uptake (i.e., $\rho N_x = \rho NO_3^- + \rho NH_4^+ + \rho urea$). We thus estimated urea uptake at the stations across the Weddell Sea where ρurea was not directly measured by multiplying $\rho NO_3^- + \rho NH_4^+$ by 0.08 (see section 3.3.4; equation 7). If anything, this will lead to an underestimate of the f-ratio and carbon export potential.

Figure and Table captions:

Table S1. Average carbon content for the various diatom species identified using Light Microscopy taken from Leblanc et al. (2012) for high latitude locations (50 – 70°S).

Diatom species	Average carbon content (pg C $cell^{-1}$)
Actinocyclis actinochilus	13575
Amphiprora kufferathi	2115
Amphora sp.	4
Asteromphalus hookeri	1893
Bacteriastrum	2376
Banquisia belgicae	-
Berkeleya rutilans	-
Chaetoceros atlanticus	463
Chaetoceros brevis/neglectus	395
Chaetoceros bulbosa	-
Chaetoceros castracanei	3247
Chaetoceros concavicornis	883
Chaetoceros convolutus	321
Chaetoceros curvatus	388
Chaetoceros debilis	355
Chaetoceros decipiens	1079
Chaetoceros dichaeta	800
Chaetoceros flexuosus	138
Chaetoceros hendeyi	404
Chaetoceros peruvianus	404
Chaetoceros simplex	254
Chaetoceros tortissimus	205
Cocconeis spp	505
Corethron pennatum	317
Coscinodiscus asteromphalus	95958
Coscinodiscus bouvet	22195
Cylindrotheca closterium	300
Dactyliosolen	9039
Entomoneis paludosa	1499
Ephemera planamembranacea	723
Eucampia antarctica var antarctica	1231
Eucampia antarctica var recta	1231
Fragilariopsis curta	55

Table S1. *continued*

Diatom species	Average carbon content (pg C cell^{-1})
Fragilariopsis kerguelensis	283
Fragilariopsis long	243
Fragilariopsis pseudonana	26
Fragilariopsis rhombica	189
Fragilariopsis richerii	243
Fragilariopsis small	26
Gyrosigma sp	5694
Haslea spp	748
Leptocylindrus mediterraneus	1450
Manguinea fusiformis	1114
Membraneis challengeri	12162
Navicula directa	2006
Navicula sp.	1999
Neocalyptrella sp	-
Nitzschia australis	4422
Nitzschia lecontei	4422
Nitzschia medioconstricta	4422
Nitzschia sicula	135
Nitzschia sp.	4422
Nitzschia stellata	4422
Odontella litigosa	4722
Odontella weisflogii	4722
Pinnularia sp	2918
Plagiotropus gaussii	3230
Pleurosigma directum	5050
Proboscia alata	2202
Proboscia inermis	3278
Proboscia sp.	2202
Pseudo-nitzschia sp1	32
Pseudo-nitzschia sp2	32
Pseudo-nitzschia subcurvata	24
Rhizosolenia	3798
Rhizosolenia imbricata	2238
Thalassionema nitzschoides	115
Thalassiosira big	2476
Thalassiosira gracilis	319
Thalassiosira lentignosa	4047
Thalassiosira small	42
Thalassiosira very big	7934
Thalassiothrix antarctica	2456
Trichotoxon reinboldii	4708

"-" indicates no available data

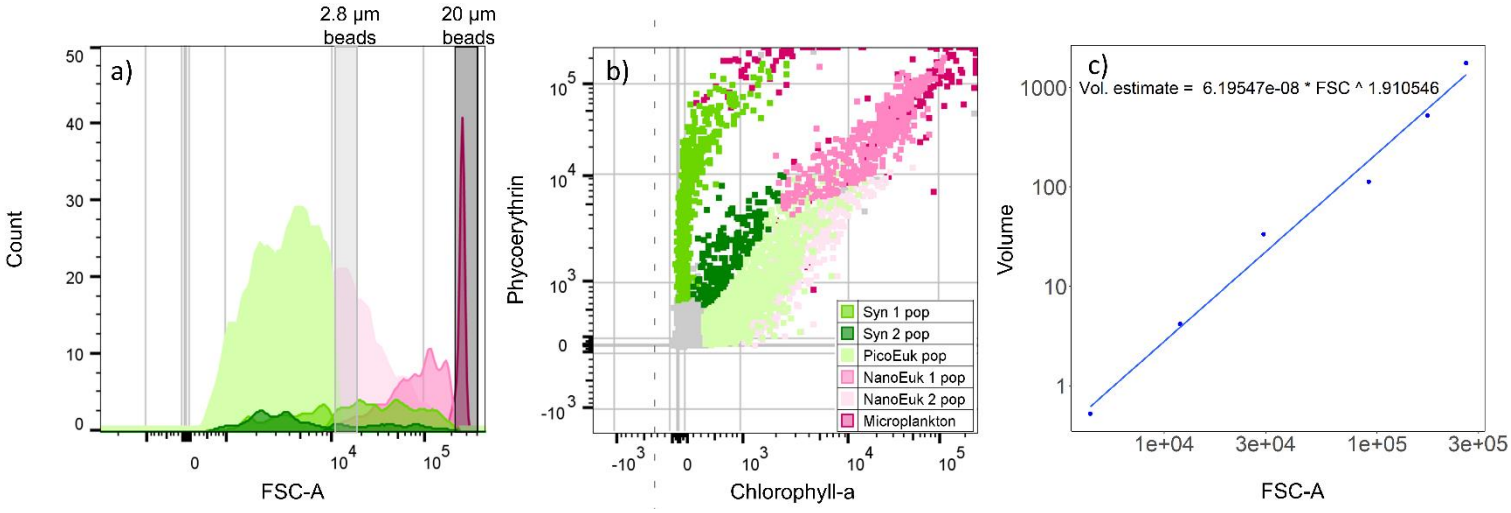

Figure S1. Example (a) histogram of relative cell size from forward scatter area (FSC-A) and (b) cytogram of phycoerythrin (i.e., orange fluorescence) on the y-axis versus chlorophyll-a (i.e., red fluorescence) on the x-axis showing the populations that were identified using flow cytometry across the Weddell Sea. Panel (c) shows the calibration curve used to calculate the biovolume of the different phytoplankton groups generated from beads of various sizes. The populations identified in the sample are as follows: *Synechococcus* (Syn 1 and Syn 2), picoeukaryotes (PicoEuks), nanoeukaryotes (NanoEuk 1 and NanoEuk 2), and microeukaryotes (MicroEuk). The grey vertical bars in panel (a) indicate the FSC-A of the 2.8 µm beads (light grey) and 20 µm beads (dark grey). The grey dots in panel (b) show background noise and detritus.

Table S2. Average biovolumes of the various phytoplankton populations identified using flow cytometry. Due to the anomalous FSC-A of the *Synechococcus* populations, the average biovolume for these populations was taken from literature (Kana and Glibert 1987; Paulsen et al. 2015).

Phytoplankton group	Average biovolume (μm^3)
Synechococcus 1	1*
Synechococcus 2	1*
Picoeukaryotes	0.7 ± 0.3
Nanoeukaryotes 1	159 ± 69
Nanoeukaryotes 2	52 ± 26
Microeukaryotes	1300 ± 29

**Taken from literature (Kana and Glibert 1987; Paulsen et al. 2015)*

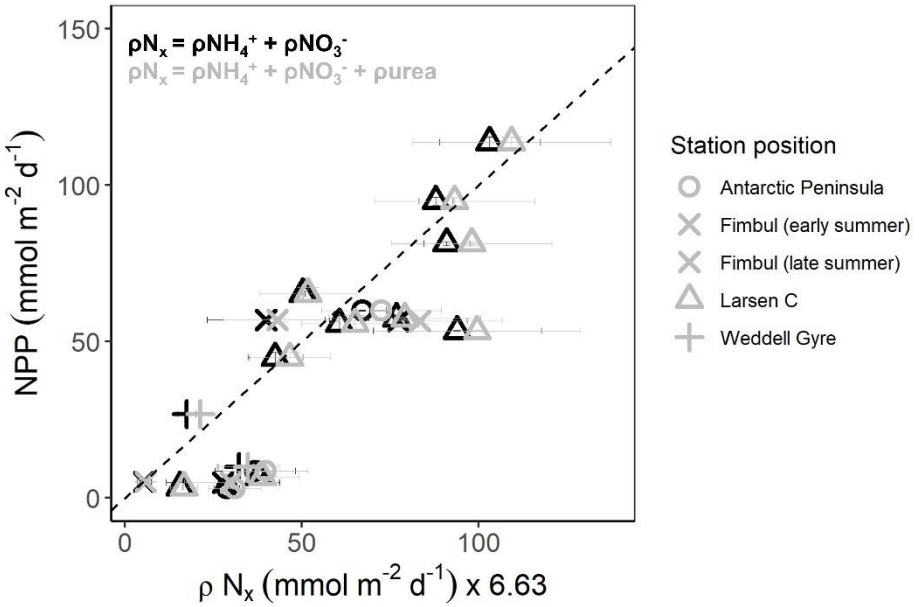

Figure S2. Euphotic zone-integrated rates of NPP and total N uptake (ρN_x) x 6.63. The black symbols represent total N uptake = ρNO_3^- + ρNH_4^+ and the grey symbols show total N uptake = ρNO_3^- + ρNH_4^+ + ρurea. The dashed line represents the 1:1 line. The error has been propagated according to standard statistical practices.

Supplemental Information References:

Leblanc, K., Armand L, Assmy P, Beker B, Bode A, Breton E, Cornet V, et al. 2012. "A Global Diatom Database – Abundance, Biovolume and Biomass in the World Ocean." *Earth System Science Data* 4: 419–165.

Kana, Todd M., and Patricia M. Glibert. 1987. "Effect of Irradiances up to 2000 ME M-2 s-1 on Marine Synechococcus WH7803-I. Growth, Pigmentation, and Cell Composition." *Deep Sea Research Part A, Oceanographic Research Papers* 34 (4): 479–95. https://doi.org/10.1016/0198-0149(87)90001-X.

Kaprelyants, A. S., and D. B. Kell. 1993. "Dormancy in Stationary-Phase Cultures of Micrococcus Luteus: Flow Cytometric Analysis of Starvation and Resuscitation." *1Applied and Environmental Microbiology* 59 (10): 3187–96.

Mdutyana, Mhlangabezi, Sandy J. Thomalla, Raissa Philibert, Bess B. Ward, and Sarah E. Fawcett. 2020. "The Seasonal Cycle of Nitrogen Uptake and Nitrification in the Atlantic Sector of the Southern Ocean." *Global Biogeochemical Cycles* 34 (7): 1–29. https://doi.org/10.1029/2019GB006363.

Paulsen, M. L., K. Riisgaard, T. F. Thingstad, M. S. John, and T. G. Nielsen. 2015. "Winter-Spring Transition in the Subarctic Atlantic: Microbial Response to Deep Mixing and Pre-Bloom Production." *Aquatic Microbial Ecology2* 76 (1): 49–49.

Peng, Xuefeng, Sarah E Fawcett, Nicolas Van Oostende, Martin J Wolf, Dario Marconi, Daniel M Sigman, and Bess B Ward. 2018. “Nitrogen Uptake and Nitrification in the Subarctic North Atlantic Ocean.” https://doi.org/10.1002/lno.10784.

Sunda, William G., and Susan A. Huntsman. 2015. “High Iron Requirement for Growth, Photosynthesis, and Low-Light Acclimation in the Coastal Cyanobacterium Synechococcus Bacillaris.” *Frontiers in Microbiology2* 6: 561.